# Giant director fluctuations in liquid crystal drops

Alexis de la Cotte,[1] Olaf Stenull,[1] Sophie Ettinger,[1] Peter J. Collings,[1,2] Tom C. Lubensky,[1] and A. G. Yodh[1]
[1]*Department of Physics and Astronomy, University of Pennsylvania, Philadelphia, Pennsylvania 19104, USA*
[2]*Department of Physics and Astronomy, Swarthmore College, Swarthmore, Pennsylvania 19081, USA*

(Received 12 December 2019; revised 11 March 2021; accepted 2 February 2022; published 5 April 2022)

We report the discovery and elucidation of giant spatiotemporal orientational fluctuations in nematic liquid crystal drops with radial orientation of the nematic anisotropy axis producing a central "hedgehog" defect. We study the spatial and temporal properties of the fluctuations experimentally using polarized optical microscopy, and theoretically, by calculating the eigenspectrum of the Frank elastic free energy of a nematic drop of radius $R_2$, containing a spherical central core of radius $R_1$ and constrained by perpendicular boundary conditions on all surfaces. We find that the hedgehog defect with radial orientation has a complex excitation spectrum with a single critical mode whose energy vanishes at a critical value $\mu_c$ of the ratio $\mu = R_2/R_1$. When $\mu < \mu_c$, the mode has positive energy, indicating that the radial hedgehog state is stable; when $\mu > \mu_c$, it has negative energy indicating that the radial state is unstable to the formation of a lower-energy state. This mode gives rise to the large-amplitude director fluctuations we observe near the core, for $\mu$ near $\mu_c$. A collapse of the experimental data corroborates model predictions for $\mu < \mu_c$ and provides an estimate of the defect core size.

DOI: 10.1103/PhysRevE.105.044702

## I. INTRODUCTION

Topological defects affect the stability and self-assembly of complex fluids such as liquid crystals (LCs) and colloids [1–4]. Much of the research done on LCs, for example, explores how defect topology, arrangement, and number vary as a function of elasticity, confinement geometry, boundary conditions, anchoring energetics, and thermodynamic phase. These studies, in turn, guide efforts to create self-organized and responsive soft materials [3,5–21]. To date, research on topological defects has predominantly explored equilibrium structure and energetics of nearby director fields. Director *fluctuations* near defects are rarely studied. Here we investigate spatiotemporal fluctuations of the nematic LC (NLC) director-field near the core of a classic hedgehog defect (topological charge $+1$) at the center of a spherical drop with perpendicular (homeotropic) director alignment at the drop surface.

Two equilibrium structural configurations are commonly observed in these NLC drops [4,11,12,23–25]: a radial hedgehog, with nematic director **n**, the unit vector specifying the direction of the nematic anisotropy axis, parallel to the pure radial coordinate, and a "twist-bend" hedgehog [26], wherein twist and bend distortions occur near the drop center. The relative stability of these two configurations has received some theoretical attention [4,11,23–25]. Reference [17] reports a transition from the radial hedgehog to a configuration featuring a hyperbolic core and a nonsingular charge $+1$ disclination ring. Another possible configuration, much studied by theory [27–33], is one in which the point core is replaced by a strength $+1/2$ disclination ring. Here we focus on director dynamics of drops with a radial hedgehog equilibrium configuration. Our model assumes drops of radius $R_2$, a central core consisting of a spherical inclusion of radius $R_1$, and homeotropic (perpendicular) boundary conditions on all surfaces. To date, director dynamics near a defect core, as opposed to defect translational diffusion [34], have not been investigated much beyond the fast fluctuations occurring on molecular scales [35–41], or the dynamics emerging from rapid lattice vibrations of skyrmions in 2D films [42].

Our measurements and theoretical analysis [43] reveal a remarkable feature of the hedgehog director configuration that has not been reported in other systems and confinement geometries [3,10,15,18,20,21]. We find that slow, giant fluctuations of the director field **n** can emerge, driven by a low-energy excitation mode strongly localized near the core, with energy eigenvalue that approaches zero at a critical value $\mu_c$ of the ratio $\mu = R_2/R_1$ (see Supplemental Material (SM), Movie 1 [22]) and becomes negative for $\mu > \mu_c$. We will refer to this low-energy excitation as the *critical* mode. The remaining modes have much higher energies and thus much smaller fluctuation amplitudes. Our calculations predict a limit of stability at $\mu = \mu_c$ that agrees with the results of Ref. [23].

Using video-rate polarized optical microscopy (POM) and image analysis, we measure the spatiotemporal fluctuations of the director **n** around the hedgehog defect and reconstruct **n** and its correlation functions. The observations reveal cooperative modes of **n** that relax diffusively at different rates. In many drops, **n** exhibits giant correlated fluctuations with amplitudes as large as $\pi/8$ rad. Experimental measurements of the temporal autocorrelation functions of **n** yield fluctuation amplitudes and decay times, and when combined with theory, provide an estimate of the size of the central core in drops with giant fluctuations. Moreover, a somewhat surprising and informative collapse of the experimental data is observed when the critical-mode energy approaches zero. Thus, the

 

combination of experiment and theory yields fresh insight into the character of **n** in the vicinity of a simple defect core. Such critical points could arise for topological defects in other confined geometries/contexts such as defects in free-standing Smectic-C films [44–50] and are potentially interesting for nanoparticles in LCs [43,47–50].

## II. EXPERIMENTAL

The experiments employ an NLC-water emulsion using a mixture of 4-*n*-pentyl-4′-cyanobiphenyl (5CB, Kingston Chemicals) that we hand-mix with a 0.1 wt% aqueous solution of the surfactant sodium dodecyl sulfate (SDS, Sigma-Aldrich). The latter promotes homeotropic anchoring at the water/NLC-drop boundary [11,12], and the hand-mixing helps minimize surfactant dispersion in the LC. The resulting emulsion consists of spherical drops of NLC of varying size, with only a few of the many suspended drops making pointlike contact with a cell wall.

The samples are imaged with POM using a Leica DM IRB inverted microscope and a 100x oil immersion objective (N.A. = 1.4). Imaging of each drop is done at 60 frames per second over a period of 5 to 10 min. The apparent softening of the radial-hedgehog ground state configuration and emergence of slow, giant, angular fluctuations of **n** are observable in POM as illustrated in Fig. 1 (top-left image) and SM Movie 1 [22]. The fluctuations in roughly 50 percent of the drops were significantly larger than the measurement random noise and, therefore, are easily observed. Herein we focus on the drops that exhibit these large fluctuations but will return to put the cases with small fluctuations into theoretical context. All fluctuating drops possess the same azimuthal pattern, in agreement with the theoretical prediction (for $\mu < \mu_c$) that the fluctuations have radial symmetry and appear the same along any line of sight. Note also, we observe giant fluctuations in drops using other surfactants (e.g., CTAB) and LCs (e.g., MBBA, 8CB, ZLI-4792). Finally, please note, our observations and those in Ref. [17] are different. The latter concerns structure rather than dynamics, involves a different LC in the vicinity of the nematic-smectic transition, and reports a transition from a radial configuration to a hyperbolic state with a large disclination ring, which is different from the twist-bend configuration we find in preliminary simulations which show a simple twist-bend hedgehog (with a possible tiny Saturn-ring at the core, see SM Fig. S3 [22] and theory paper [43] for details).

Two coexisting collective diffusion modes of **n** are readily distinguished: (i) "azimuthally uniform" rotational diffusion, which varies with the radial coordinate $r$ but not with the azimuthal coordinate $\varphi$, and (ii) scissorlike "relative" rotational diffusion, which varies with both $r$ and $\varphi$, see Fig. 1 (top-right). To quantify these modes further, each video frame is analyzed. First, we employ image processing tools to locate the defect position, *i.e.*, the center of the cross-pattern. The defect position is then used to obtain an azimuthal intensity profile $I(\varphi, t)$ on a circle of probing radius $r = r_1 \approx 0.4\ \mu m$ (see Fig. 1, lower panel; SM Fig. S1 [22]).

Since the images are recorded using crossed-polarizers, the intensity profiles provide information about the director orientation at each point on the probing circle. While director orientation varies in all three spatial dimensions, we make the approximation that the observed fluctuations are contained in the $xy$ plane; angular fluctuations in the $z$ direction (along the path of the light) are difficult to quantify experimentally. To extract information, we model the system as a 2D slice, and we split each frame into eight angular regions divided by neighboring extrema (SM Fig. S1 [22]). Each region comprises and is bounded by one intensity maximum and one minimum. With the crossed polarizer setup, we can identify every local minimum as a point where the director lies parallel to one of the polarizers, and every local maximum as a point where the director makes a 45° angle with the polarizers. For other points at arbitrary angle $\varphi$ (with respect to horizontal axis), the director angle, $\beta$ (with respect to the horizontal axis, see the inset in the lower panel of Fig. 1), can be determined using the following equation: $\beta(\varphi, t) = \frac{1}{2}\arcsin\left(\sqrt{\frac{I(\varphi,t)-I_{\min}(t)}{I_{\max}(t)-I_{\min}(t)}}\right)$. Knowing $\beta$ and $\varphi$ enables us to reconstruct the orientation of the director at each value

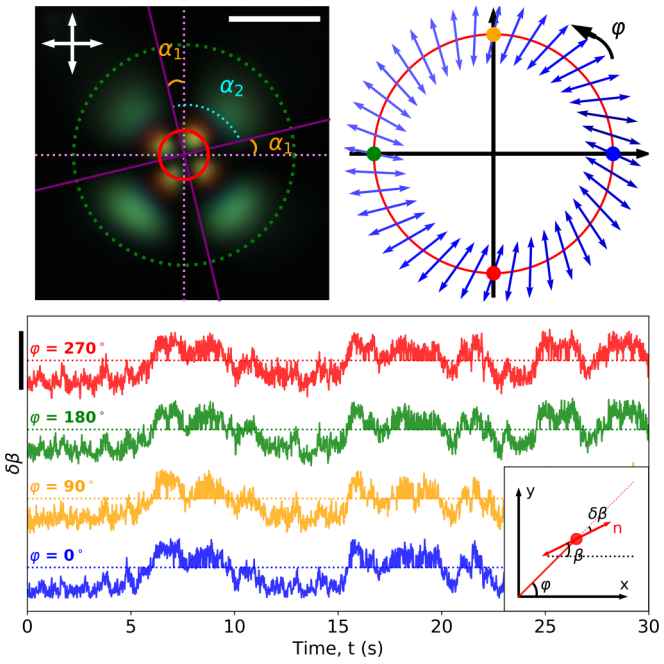


FIG. 1. Top-left: Snapshot of a fluctuating drop. "Azimuthally uniform" rotational diffusion is characterized by the angle $\alpha_1$ (centered around zero), and "relative" or scissorlike rotational diffusion is characterized by the angle $\alpha_2$ (centered around $\pi/2$). Green dashes indicate the drop outer edge. The red circle is at $r = r_1 \approx 0.4\ \mu$m. Scale bar represents 5 $\mu$m. Top-right: Reconstruction of the director **n** from the snapshot. The azimuthal intensity profile is determined along the red circle (shown also in the top-left panel). The intensity variation obtained in the crossed polarizer setup is used to extract the director angle ($\beta$, see lower panel) for each angle $\varphi$. The corresponding colored dots indicate the azimuthal positions at which the angular fluctuations shown in the lower panel are taken. Bottom: Time evolution of $\delta\beta$ at $r = r_1 \approx 0.4\ \mu m$ for four azimuthal angles, $\varphi = 0°$, 90°, 180°, and 270° (see colored dots in the top-right panel), taken along the red circle shown in the panels above. Scale bar on the $\delta\beta$ axis represents $\pi/4$ radians. Inset: Definitions of the angles $\varphi$, $\beta$, and $\delta\beta$; the $xyz$-coordinate system is defined with $z$ axis pointing out of the page.

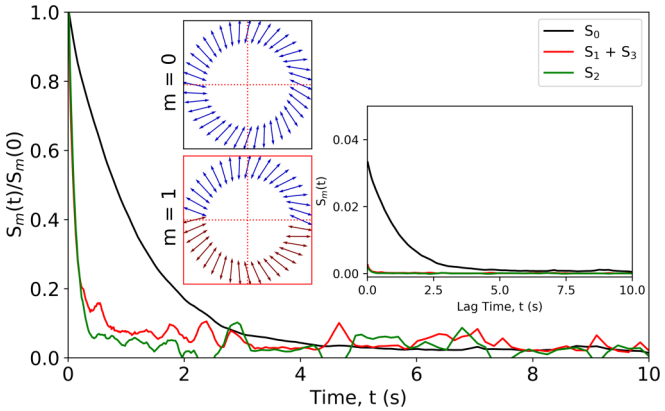


FIG. 2. Normalized and bare (inset, right) correlation functions at probing radius $r = r_1 \approx 0.4\ \mu m$. Additional insets: schematic reconstructions of **n** illustrating key features of the two coexisting fluctuation modes. Blue (red) arrows indicate positive (negative) $\delta\beta$. Notice, the $m = 0$ mode has substantially larger amplitude and relaxation time than all other modes.

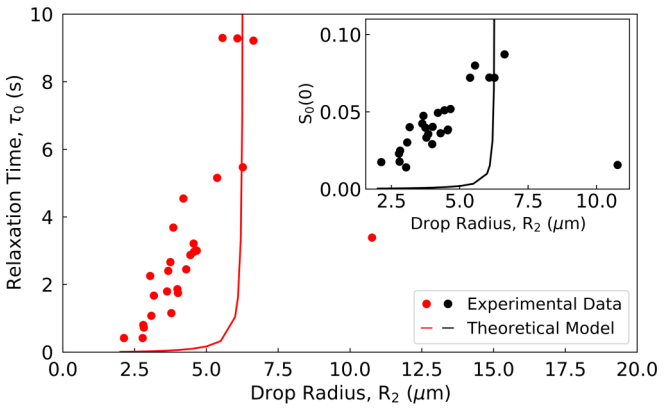


FIG. 3. Relaxation time $\tau_0$ and amplitude $S_0(0)$ (inset) at probing radius $r = r_1 \approx 0.4\ \mu$m versus drop radius, $R_2$. Solid lines are obtained using the theoretical model with a fixed core radius of $R_1 = 9.0$ nm, and the viscous parameter $\Gamma = 15\ \frac{\text{ms}}{\text{kg}}$. Notice the poor agreement between this model with fixed core radius and the experiment.

of $\varphi$, and to measure $\delta\beta(\varphi, t) = \beta(\varphi, t) - \varphi$, the deviation of **n** from the radial hedgehog ground state. Figure 1 (bottom) shows the fluctuations of $\delta\beta$ for different discrete azimuthal positions, $\varphi$. Spatiotemporal director fluctuations within the drop are shown in real time in SM, Movie 1 [22].

## III. RESULTS

Using these measurements of director fluctuations, we next build correlation functions based on $\delta\beta(r, \varphi, t)$ (the polar angle $\theta$ is fixed at its equatorial value of $\pi/2$) at discrete azimuthal angles:

$$C_p(r, t) = \left\langle \delta\beta(r, \varphi_0, t_0)\delta\beta\left(r, \varphi_0 + \frac{2\pi p}{N}, t_0 + t\right)\right\rangle, \quad (1)$$

with $p = 0, 1, \ldots, N-1$. These correlations are averaged over angular position $\varphi_0$ and time $t_0$. We set $N$ to 4 since the POM image provides a cross pattern with four identifiable branches (Fig. 1). The data are then further processed by performing a discrete Fourier transform of $C_p(r, t)$:

$$S_m(r, t) = \frac{1}{N}\sum_{p=0}^{N-1} C_p(r, t)\exp\left(-im\frac{2\pi p}{N}\right). \quad (2)$$

Reality of $C_p(r, t)$ requires $S_0(r, t)$ and $S_2(r, t)$ to be real, and $S_1(r, t)$ and $S_3(r, t)$ to be complex conjugates of each other. Figure 2 shows an example of the correlation functions $S_0$, $S_2$ and $S_1 + S_3$ versus time, using the measurements of $\delta\beta$ shown in Fig. 1. Since our measurements are mostly made at a specific $r$, herein, we drop the $r$-dependence in $S_m$ and $C_m$.

Fourier transformation decomposes the fluctuations into modes with different azimuthal dependence. Based on Eq. 2, $S_{m=0}$ corresponds to a sum of all $C_p(r, t)$; it characterizes the "azimuthally uniform" rotational diffusion, and its value is large when similar (in-phase) fluctuations occur at all $\phi$. $S_{1,3} \equiv S_1 + S_3 = 2\text{Re}S_1 = (C_0 - C_2)/2$, characterizes the "relative" rotational diffusion by looking at "opposing" or "out-of-phase" (scissorlike) fluctuations for positions separated by 180°. Clear differences are apparent between modes $S_0$ and $S_{1,3}$. First, the amplitude, $S_0(0)$, is approximately one order of magnitude larger than $S_{1,3}(0)$, indicating the dominance of the lowest-order-mode fluctuations of **n** (inset, Fig 2). Second, the relaxation time $\tau_0$ is ≈1 s, while $\tau_{1,3}$ is very short, about the time between video frames (≈0.017 s).

For the remainder of this paper, we focus on the fluctuations, $S_0(t)$, of the dominant, critical mode. The dependence of its amplitude, $S_0(0)$, and relaxation time, $\tau_0$, is shown in Fig. 3 as a function of drop radius ($R_2$). These plots include only drops with $S_0(0)$ larger than the measurement noise floor [$S_0(0) > 0.01$]. An increasing trend for both amplitude and relaxation time with drop size is apparent for radii $R_2 < 7.5\ \mu$m. $S_0(t)$ and $\tau_0$ as a function of lag time, and for different values of $r$ within the drop, are shown in Fig. S2; these measurements reveal an expected suppression of $S_0(0)$ with increasing $r$, and a $\tau_0$ that is constant within experimental error for all $r$.

## IV. DISCUSSION

In our theory, of which we give a detailed account in a dedicated publication [43], we describe the energetics of our drops based on the usual Frank free energy,

$$F = \frac{1}{2}\int \{K_1(\nabla\cdot\mathbf{n})^2 + K_2(\mathbf{n}\cdot\nabla\times\mathbf{n})^2 + K_3[\mathbf{n}\times(\nabla\times\mathbf{n})]^2\}d^3r. \quad (3)$$

The splay, twist, and bend elastic constants, are set to standard values for 5CB: $K_1 = 6.4$, $K_2 = 4.0$, $K_3 = 10.0$, all in $pN$. The equilibrium director aligns everywhere along the radial direction: $\mathbf{n}_0 = \hat{e}_r$. To study fluctuations about this state, we express the local director as

$$\mathbf{n} = \sqrt{1 - f^2 - g^2}\hat{e}_r + f\hat{e}_\phi + g\hat{e}_\theta = \mathbf{n}_0 + \delta\mathbf{n}, \quad (4)$$

where, as in previous work [23,43], $f$ and $g$ are functions of radius $r$ and polar angle $\theta$ and, importantly, are also functions of the azimuthal angle $\varphi$. We determine the modes associated with $f$ and $g$ by standard separation-of-variable methods with product-function solutions [43]. The polar-angle functions obey a Legendre equation of irrational order, and the

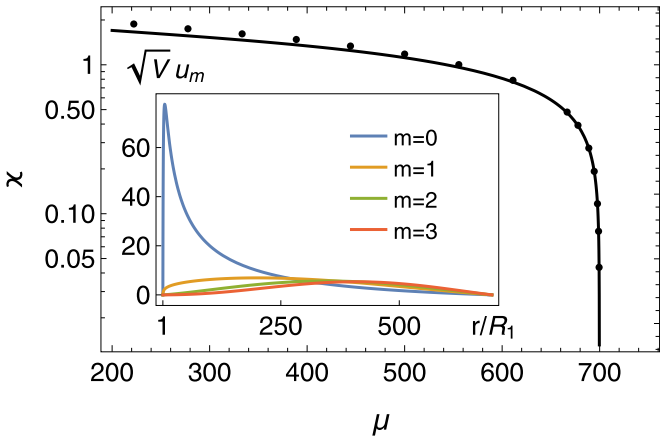


FIG. 4. Numerical results (dots) and analytical approximation (solid line) for the smallest allowed $\kappa(\mu)$ associated with the critical mode (for $\mu < \mu_c$) that has radial eigenfunction $u_0(r)$. Inset: examples of radial $f$-eigenfunctions $u_m$ for a drop with $\mu = R_2/R_1 \approx 695$. Notice, $u_0(r)$ is strongly peaked near the core. $V$ is the total volume of the drop given by $V = (4/3)\pi R_2^3$.

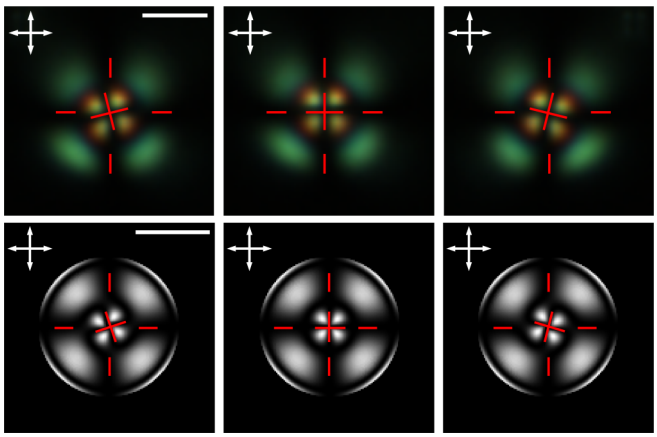

FIG. 5. Comparison of three images of an actual drop showing the fluctuations (top row), and three reconstructed polarized microscopy images predicted by the theory, calculated using the Jones Matrix formalism (bottom row). The scale bars represent 5 $\mu$m. Since refraction at the drop surface is not taken into account, the agreement between the images and theoretical reconstructions is best for small values of the radial coordinate, e.g., inside the dark circle where the retardation equals $2\pi$.

radial functions obey a Bessel equation of real or imaginary irrational order.

Each solution, which is constructed so that the critical mode wave function and associated fluctuations vanish at $r = R_1$, is characterized by a parameter,

$$\kappa = kR_2, \tag{5}$$

where $k$ is the exact analog of the wave number in a plane-wave system; $k$ takes on an infinite set of discrete values such that wave functions vanish at the outer boundary at radial position $r = R_2$. The energy density of eigenmodes is determined by $\kappa$ via

$$\varepsilon = K_3\left(\frac{\kappa}{R_2}\right)^2. \tag{6}$$

Importantly, $\kappa$, and thus the zeros of the radial solutions, depend on the ratio $\mu = R_2/R_1$, rather than on $R_1$ and $R_2$ separately. The lowest energy configuration associated with each mode corresponds to the smallest allowed values of $\kappa$. For $\mu < \mu_c$, the radial eigenfunction of the lowest energy excitation, $u_0(r)$, is strongly peaked near the core, whereas all the other excitations are much less localized; see Fig. 4. When $\mu > \mu_c$, $\kappa$ becomes imaginary, and $\epsilon_0$ becomes negative, indicating an instability with respect to a nonradial state.

The theoretical solution (for $\mu < \mu_c$) is used to generate instantaneous director configurations for comparison to experimental images. The dark and bright regions observed through crossed-polarizers are readily explained using the 5CB birefringence. Light traveling through the dark ring/annulus at approximately $r = R_2/3$ experiences a retardation of $2\pi$; the colors in the bright regions are different because the birefringence has dispersion. We then utilize Jones calculus to calculate the optical transmission through the full three-dimensional drop and crossed polarizers, i.e., based on the theoretical director configuration. Since refraction at the drop surface is not taken into account, the reconstructed images are only approximate for values of $r$ approaching $R_2$. Figure 5 displays both the theoretical reconstructions and the experimental images. The visual correspondence between theory and experiment in the center portion of the drop is excellent. Importantly, the fluctuations are largest near the core, consistent with the prediction that $u_0(r)$ is sharply peaked near the core.

Our theory [43] provides insight into the character of the lowest-energy excitation mode. In particular, it provides us with an analytic expression for small values of $\kappa^2$ as a function of $\mu$, and it determines the critical value, $\mu_c = e^{i\pi/\nu} \approx 700$ for 5CB, at which $\kappa$ vanishes. Here $\nu$ is the order of the Bessel equation for the radial eigenfunction of the lowest-energy mode. Figure 4 plots $\kappa$ as a function of $\mu$.

For in-depth comparison with experiment, we compute the static and dynamic correlation functions via standard Gaussian functional integrations with $F$ expressed in terms of its eigenfunctions [43,51]. Because our experimental analysis uses a 2D slice approximation and thus derives experimental information about only azimuthal fluctuations of the director, we need only the azimuthal deviation, $f \approx \delta\beta$, to build theoretical correlation functions for experimental comparison. Our theoretical model predicts

$$S_0(r,t,\mu) = \frac{3k_BTu_0^2(r,\mu)}{8\pi\epsilon_0(\mu)}e^{-t/\tau_0(\mu)}, \quad \tau_0(\mu) = \frac{1}{\Gamma\varepsilon_0(\mu)}, \tag{7}$$

where the 0 subscript denotes the lowest energy state and $\Gamma$ is the viscous parameter for the LC, i.e., the inverse rotational viscosity of the liquid crystal, $\gamma_1$. For 5CB, electro-optical measurements [52] give $\gamma_1 \approx 0.07$ Pa-s, and hence $\Gamma \approx 15\ \frac{\text{ms}}{\text{kg}}$ at room temperature. Note, $S_0$ is proportional to $\varepsilon_0^{-1}$, and as a result diverges as $\mu$ approaches $\mu_c$. In Eq. (7), we explicitly indicate that $\varepsilon_0$, $u_0$, and $\tau_0$ depend on $\mu$, the sole free variable once $\kappa$ is replaced by its analytic expression in terms of $\mu$. Our measurements are generally taken at radius $r = R_2/3$. A complete analysis demonstrates that higher-order modes

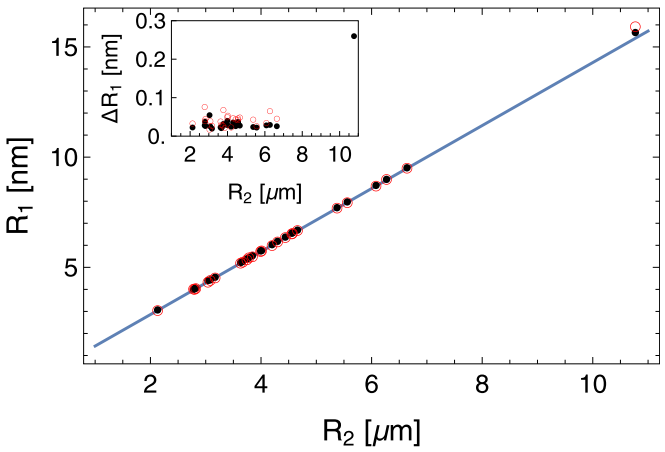


FIG. 6. Size of the core radius $R_1$ extracted from the experimental values of $S_0$ (black dots) and $\tau_0$ with $\Gamma = 20\ \frac{\text{ms}}{\text{kg}}$ (red open circles). The solid line is the critical line, Eq. (8), highlighted by the theory. Inset: deviation $\Delta R_1 = R_1 - R_2/\mu_c$ of the experimental points from the critical hedgehog.

have much larger energies, much smaller amplitudes, and much shorter relaxation decay times than does the lowest mode. These predictions thus agree with our observations of the rapidly decaying and small amplitude scissorlike modes (Fig. 2).

Our observation of some drops with visible central water droplets, and prior theoretical work showing that the radial director configuration is not stable without anchoring of the director near the center [11,23], strongly suggest that all of the drops we studied house a central water droplet. The central droplet position is easily identified as the center of a black cross defining the boundaries of the four-arm polarization pattern (see Fig. 5), but its size (radius) is too small to be detected by our optical techniques, thereby precluding any possibility of a direct measurement of the core radius $R_1$. Our hand-mixing process is likely to produce drops with varying core sizes, since varying amounts of water and surfactant can become trapped inside the drops and migrate to their centers. Indeed, attempts to fit Eq. (7) to our data for $S_0(r, 0, \mu)$ and $\tau(\mu)$ versus $R_2$, with a single $R_1$ as a fitting parameter, lead to poor agreement between experiment and theory (Fig. 3). Therefore, to study core size, we use our theoretical results to calculate $R_1$, first using $S_0(r, 0, \mu)$ and then using $\tau_0(\mu)$. In the first case, all parameters except $\mu$ are fixed. By setting $S_0(r, 0, \mu)$ equal to the experimentally determined values of this quantity, we obtain an equation determining $\mu$ for each value of $R_2$ from which we obtain $R_1 = R_2/\mu$. The values of $\mu$ obtained in this way differ from $\mu_c$ by an order of one percent (or less) implying that $R_1$ differs from

$$R_1 = \frac{R_2}{\mu_c} \tag{8}$$

by the same small percentage. Figure 6 shows the strikingly linear plot of $R_1$ versus $R_2$ and the small deviation of $R_1$ from Eq. (8). This behavior is a consequence of the fact that we are only able to detect large fluctuations, which only arise when $\varepsilon_0$ is near zero, i.e., when $\mu$ is near $\mu_c$.

The calculation of $\mu$ from $S_0(r, 0, \mu)$ is a straightforward task (with the help of Mathematica) because it has no unknowns other that the $\mu$ we seek to solve for. The function $\tau_0$, which does not depend on the wave function $u_0$, is less complex than that for $S_0$, but it also depends on the viscous parameter $\Gamma$ whose value we do not know. We have two options for extracting $\mu$ from $\tau$: (i) We can use $\Gamma$ as a fit parameter. In this case, it turns out that the resulting dependence of $R_1$ on $R_2$ is remarkably insensitive to the value $\Gamma$; any value larger than roughly 10 $\frac{\text{ms}}{\text{kg}}$ leads to essentially the same outcome. (ii) We can extract $\Gamma$ for each $R_2$ from the ratio $S_0(r, 0, \mu)/\tau_0(\mu)$ using Eq. (4) and the known values of $T$ and $u_0^2(r)$. In the latter case, we find $\Gamma = 28.9 \pm 9.6\ \frac{\text{ms}}{\text{kg}}$; note, the scatter is not large enough to alter the functional dependence of $R_1$ on $R_2$. Ultimately, both the data sets for $S_0(r, 0, \mu)$ and $\tau_0(\mu)$ lead to highly consistent estimates for $R_1$ as a function of $R_2$ (see Fig. 6).

Our analysis suggests that $R_1$ varies from approximately 5 to 25 nm, albeit with most cores between 5 and 12 nm. These numbers are comparable to those found in other analyses of defect cores [53–55], and are consistent with recent experimental insights about the nanostructure of topological defects [28] and theoretical work on the structure of nematic hedgehogs [27,31,56].

Measurements of director fluctuations are easy near $\mu = \mu_c$ because of their large amplitude, but they become difficult away from that point, when the director fluctuation amplitudes become comparable to the experimental noise floor. In some drops with diameters in the 5–10 micron range, the core radii were measurable and were in the 550–750 nm range ($\mu \approx$ 7–20); notably, these drops did not show giant fluctuations, consistent with their value of $\mu \ll \mu_c$.

However, approximately 50% of drops in our study, largely with diameters in the 3–6 micron range, have cores too small to be seen and did not exhibit measurable fluctuations. For these drops, theory suggests that either $\mu \leqslant 0.85\mu_c$, i.e., $\mu$ lies on the plateau, or, $\mu > \mu_c$. Clearly, it is desirable to develop a better understanding of the drops director configuration when $\mu > \mu_c$. To this end, we have begun a study [57] using Q-based Landau-de Gennes (LdG) numerical models [58–61] of the ground-state configurations of our system as a function of Frank elastic constants and the ratio $\mu$. Preliminary results, based on simulated drops smaller than those in experiment, confirm that a radial hedgehog is the lowest energy configuration for $\mu < \mu_c$. We find a lowest-energy state that is a twisted hedgehog (with a possible tiny Saturn-ring at the core) at $\mu$ greater than but very near $\mu_c$ and more complex twisted structures as $\mu$ grows larger. The radial hedgehog and twist-bend hedgehog configurations are pictured in SM Fig. S3 [22], and the simulations will be discussed in detail in a future paper [57]. As noted earlier, twisted equilibrium states have been predicted in NLC drops with and without [12,13,17] spherical cores with a range of values for the Frank constants, and twisted equilibrium states have also been observed experimentally in LC drops [11,12,23–25], albeit in larger drops than studied here.

Our experiments found no evidence of the twisted equilibrium configuration. We suspect this a consequence of the preparation method used to create the drops. For example, if handshaking/mixing tends to produce drops containing an

amount of water/surfactant roughly proportional to the drop volume, then the radius of the core could scale with the drop radius, limiting the observable range of $\mu = R_2/R_1$ to values below $\mu_c$ wherein the radial configuration is stable. Thus, we speculate that drops with $\mu > \mu_c$ may never have been created.

## V. CONCLUSION

In summary, collective fluctuation modes of **n**, and their diffusive relaxation, are reported for the first time in NLC drops. *Slow and giant fluctuations* of the lowest-energy (critical), in-phase rotational mode are observed by POM in the vicinity of a point defect. Both the amplitude and relaxation time of these fluctuations are orders of magnitudes larger than the usual fluctuations in NLCs. Our theoretical analysis suggests important new features about the character of the critical mode. Giant fluctuations arise because the energy of the lowest excitation approaches zero as the ratio $\mu = R_2/R_1$ increases, leading to a softening of the director configuration near the core, presaging a critical mode phase transition to a twisted state. The characteristic features of this mode are apparent in a remarkable scaling of the data. The new understanding about this critical mode enables indirect measurement of core size, suggests the possible existence of similar dynamical effects near other topological defects in different geometries/contexts, and offers new routes to probe local properties of topological defects and the physics of nanometer-size particles in LCs.

## ACKNOWLEDGMENTS

This work was supported by the NSF (Grant No. DMR20-03659), the PENN MRSEC (Grant No. DMR17-20530), including its Optical Microscopy Shared Experimental Facility, and NASA (Grant No. 80NSSC19K0348). We thank Angel Martinez and Wei-Shao Wei for fruitful conversations, and we thank Analisa Hill and Zoey Davidson for programming help.

[1] P.-G. de Gennes and J. Prost, *The Physics of Liquid Crystals*, 2nd ed. (Oxford Science Publications, Oxford, UK, 1993).
[2] P. M. Chaikin and T. C. Lubensky, *Principles of Condensed Matter Physics* (Cambridge University Press, Cambridge, UK, 1995).
[3] M. Kleman and O. D. Lavrentovich, Philos. Mag. **86**, 4117 (2006).
[4] H. Stark, Phys. Rep. **351**, 387 (2001).
[5] P. J. Collings and J. W. Goodby, *Introduction to Liquid Crystals: Chemistry and Physics*, 2nd ed. (CRC Press, Boca Raton, FL, 2019).
[6] P. Drzaic, *Liquid Crystal Dispersions* (World Scientific, Singapore, 1995).
[7] M. Kleman, *Points, Lines, and Walls: In Liquid Crystals, Magnetic Systems, and Various Ordered Media* (Wiley, New York, NY, 1983).
[8] J. H. Erdmann, S. Žumer, and J. W. Doane, Phys. Rev. Lett. **64**, 1907 (1990).
[9] T. Lopez-Leon, V. Koning, K. B. S. Devaiah, V. Vitelli, and A. Fernandez-Nieves, Nat. Phys. **7**, 391 (2011).
[10] T. Lopez-Leon and A. Fernandez-Nieves, Colloid Polym. Sci. **289**, 345 (2011).
[11] P. Poulin, H. Stark, T. C. Lubensky, and D. A. Weitz, Science **275**, 1770 (1997).
[12] P. Poulin and D. A. Weitz, Phys. Rev. E **57**, 626 (1998).
[13] T. C. Lubensky, D. Pettey, N. Currier, and H. Stark, Phys. Rev. E **57**, 610 (1998).
[14] J. Jeong, Z. S. Davidson, P. J. Collings, T. C. Lubensky, and A. G. Yodh, Proc. Natl. Acad. Sci. USA **111**, 1742 (2014).
[15] J. Jeong, L. Kang, Z. S. Davidson, P. J. Collings, T. C. Lubensky, and A. G. Yodh, Proc. Natl. Acad. Sci. USA **112**, E1837 (2015).
[16] G. E. Volovik and O. D. Lavrentovich, Sov. Phys. JETP **58**, 1159 (1983).
[17] O. D. Lavrentovich and E. M. Terent'ev, Sov. Phys. JETP **64**, 1237 (1986).
[18] P. W. Ellis, S. Huang, S. Klaneček, J. Vallamkondu, E. Dannemiller, M. Vernon, Y. Chang, P. M. Goldbart, and A. Fernandez-Nieves, Phys. Rev. E **97**, 040701(R) (2018).
[19] P. W. Ellis, K. Nayani, J. P. McInerney, D. Z. Rocklin, J. O. Park, M. Srinivasarao, E. A. Matsumoto, and A. Fernandez-Nieves, Phys. Rev. Lett. **121**, 247803 (2018).
[20] S.-H. Chen and B. J. Liang, Appl. Phys. Lett. **59**, 1173 (1991).
[21] H.-S. Kitzerow, Liq. Cryst. **16**, 1 (1994).
[22] See Supplemental Material at http://link.aps.org/supplemental/10.1103/PhysRevE.105.044702 for details on the experimental methodology, numerical simulations and an illustrating movie of the fluctuations.
[23] A. Rüdinger and H. Stark, Liq. Cryst. **26**, 753 (1999).
[24] M. J. Press and A. S. Arrott, Phys. Rev. Lett. **33**, 403 (1974).
[25] M. J. Press and A. S. Arrott, J. Phys. Colloques **36**, C1-177 (1975).
[26] Ref. [23] refers to this as a twist state. We prefer "twist-bend" state, because twist necessarily produces bend. See Ref. [43].
[27] S. Kralj and E. G. Virga, J. Phys. A: Math. Gen. **34**, 829 (2001).
[28] X. Wang, Y.-K. Kim, E. Bukusoglu, B. Zhang, D. S. Miller, and N. L. Abbott, Phys. Rev. Lett. **116**, 147801 (2016).
[29] R. Cohen and M. Taylor, Commun. Partial Diff. Eq. **15**, 675 (1990).
[30] A. Sonnet, A. Kilian, and S. Hess, Phys. Rev. E **52**, 718 (1995).
[31] C. Chiccoli, P. Pasini, F. Semeria, T. J. Sluckin, and C. Zannoni, J. Phys. II (France) **5**, 427 (1995).
[32] E. C. Gartland and S. Mkaddem, Phys. Rev. E **59**, 563 (1999).
[33] S. Mkaddem and E. C. Gartland, Phys. Rev. E **62**, 6694 (2000).
[34] C. D. Muzny and N. A. Clark, Phys. Rev. Lett. **68**, 804 (1992).
[35] G. Durand, L. Leger, F. Rondelez, and M. Veyssie, Phys. Rev. Lett. **22**, 1361 (1969).
[36] M. Vilfan, I. D. Olenik, A. Mertelj, and M. Čopič, Phys. Rev. E **63**, 061709 (2001).

[37] M. Vilfan, A. Mertelj, and M. Čopič, Phys. Rev. E **65**, 041712 (2002).
[38] S.-J. Kim, S.-I. Back, B. Lev, and J.-H. Kim, J. Phys. Soc. Jpn. **85**, 074601 (2016).
[39] P.-G. de Gennes, Mol. Cryst. **7**, 325 (1969).
[40] J. R. Kelly and P. Palffy-Muhoray, Phys. Rev. E **55**, 4378 (1997).
[41] P. Ziherl, M. Vilfan, and S. Žumer, Phys. Rev. E **52**, 690 (1995).
[42] A. Nych, J. Fukuda, U. Ognysta, S. Žumer, and I. Muševic, Nat. Phys. **13**, 1215 (2017).
[43] O. Stenull, A. de la Cotte, S. Ettinger, P. J. Collings, A. G. Yodh, and T. C. Lubensky, Phys. Rev. E **105**, 044703 (2022).
[44] O. Stenull and T. C. Lubensky, Crystals **12** (2022), doi:10.3390/cryst12010001.
[45] C. Y. Young, R. Pindak, N. A. Clark, and R. B. Meyer, Phys. Rev. Lett. **40**, 773 (1978).
[46] C. Bohley and R. Stannarius, Soft Matter **4**, 683 (2008).
[47] K. Harth and R. Stannarius, Front. Phys. **8**, 112 (2020).
[48] C. S. Rosenblatt, R. Pindak, N. A. Clark, and R. B. Meyer, Phys. Rev. Lett. **42**, 1220 (1979).
[49] K.-K. Loh, I. Kraus, and R. B. Meyer, Phys. Rev. E **62**, 5115 (2000).
[50] P. V. Dolganov and P. Cluzeau, Phys. Rev. E **90**, 062501 (2014).
[51] Reference [23] carried out a calculation similar to ours focusing on the stability of the radial hedgehog state. It did not, however, calculate the eigenvalues and eigenfunctions needed to interpret the new experimental data.
[52] S.-T. Wu and C.-S. Wu, Phys. Rev. A **42**, 2219 (1990).
[53] D. Svenšek and S. Žumer, Phys. Rev. E **66**, 021712 (2002).
[54] R. Repnik, L. Mathelitsch, M. Svetec, and S. Kralj, Eur. J. Phys. **24**, 481 (2003).
[55] N. Schopohl and T. J. Sluckin, J. Phys. (France) **49**, 1097 (1988).
[56] F. Greco and G. Marruci, Mol. Cryst. Liq. Cryst. Sci. Technol., Sect. A **210**, 129 (1992).
[57] S. Ettinger, O. Stenull, P. J. Collings, A. de la Cotte, T. C. Lubensky, and A. G. Yodh (unpublished).
[58] M. Ravnik and S. Žumer, Liq. Cryst. **36**, 1201 (2009).
[59] D. M. Sussman and D. A. Beller, Front. Phys. **7**, 204 (2019)
[60] www.alglib.net
[61] D. A. Beller, *Controlling Defects in Nematic and Smectic Liquid Crystals Through Boundary Geometry*, Ph.D. thesis (University of Pennsylvania, 2014).